

A. BURBELKO*[#], D. GURGUL*, E. GUZIK*, W. KAPTURKIEWICZ*

CELLULAR AUTOMATON SIMULATION FOR VOLUME CHANGES OF SOLIDIFYING NODULAR CAST IRON

MODELOWANIE METODĄ AUTOMATU KOMÓRKOWEGO ZMIAN OBJĘTOŚCI PODCZAS KRZEPNIĘCIA ŻELIWA Z GRAFITEM KULKOWYM

Volume changes of the binary Fe-C alloy with nodular graphite were forecast by means of the Cellular Automaton Finite Differences (CA-FD) model of solidification. Simulations were performed in 2D space for differing carbon content. Dependences of phase density on temperature were considered in the computations; additionally density of the liquid phase and austenite were deemed as a function of carbon concentration. Changes of the specific volume were forecast on the base of the phase volume fractions and changes of phase density. Density of modeled material was calculated as weighted average of densities of each phase.

Keywords: ductile iron, solidification modeling, specific volume change

W pracy przedstawiono wyniki symulacji zmian gęstości żeliwa sferoidalnego w układzie dwuskładnikowym Fe-C, wykorzystując do tego celu model oparty na metodzie automatu komórkowego i różnic skończonych. Symulacje wykonane były dla dwuwymiarowej przestrzeni dla różnych zawartości węgla. Zmiany gęstości wszystkich faz uwzględniano jako zależności temperaturowe. Dodatkowo dla cieczy i austenitu uwzględniono też zależność gęstości od zawartości węgla. Przy obliczaniu zmian objętości właściwej układu brano pod uwagę gęstości poszczególnych faz oraz ich udział objętościowy.

1. Introduction

Ductile iron (DI) has major application in critical engineering parts due to its mechanical properties and castability. The mechanical and physical properties of this material depend on the shape and number of the graphite grains and microstructure of the metallic matrix. One of the important processing characteristics for the manufacturing of the DI castings is the density changes during solidification [1-5].

Density of the majority of known materials increases during solidification. It means that volume of the solid will be smaller than the initial liquid phase. In foundry engineering it causes the need of using the feeding systems in order to eliminate the shrinkage defects.

The exception to this rule is, for example, water and bismuth. Volume of these substances increases during crystallization due to specific structure of the crystal lattice. Similarly to water and bismuth the DI may behave under a certain conditions. The reason for the volume increase during the cast iron solidification (DI as well as gray cast iron – GCI) is precipitation of the

graphite, which density is almost three times smaller than other phases. However, practical foundry knowledge shows that obtaining “healthy” casting, without shrinkage defects, made of DI is very difficult, especially for small values of the casting’s thermal module (under about 12 mm) [6].

It is known that expansion of DI is a few times greater than cast iron with flake graphite [5]. As a result of increase in volume, caused by precipitation of graphite in initial stage of crystallization, the metallostatic pressure can rise [7]. If the casting mold is not rigid enough it may lead to irreversible deformation of its walls (swelling of the mold) [2]. The increase in volume of mold cavity, due to swelling, is considered one of the reasons for forming of the shrinkage defects in DI castings solidifying in “vulnerable” molds.

Conditions of graphite growth in DI differ considerably from other grades of cast iron. In GCI both primary and eutectic graphite is in the permanent contact with parent liquid phase. Additionally, eutectic graphite – during crystallization – grows in conditions of constant contact of three phases.

* AGH UNIVERSITY OF SCIENCE AND TECHNOLOGY, AL. A. MICKIEWICZA 30, 30-059 KRAKOW, POLAND

Corresponding author: abur@agh.edu.pl

In DI globules of primary and eutectic graphite, in initial stage of crystallization, do not have the connection with austenite grains and grow directly from the liquid [4,8]. Growing graphite particles deplete the liquid of its carbon. This results in the rapid growth of the austenite dendrites branches in the direction of graphite globules. After physical contact the austenite envelopes and isolates the graphite globules from the liquid. After that the graphite particles can grow only by the diffusion of carbon from the liquid through the austenite shell. Probably this is the reason for shrinkage phenomena in DI castings to be more complicated than in other casting alloys.

Industrial castings, made of DI, are characterized by the same, known from literature, shrinkage defects typical for this alloy [2]:

- 1) the mechanism of feeders performance is far more complicated than in alloys which have no expansion; sometimes elimination of the feeders causes decrease in porosity;
- 2) minimal porosity occurs in eutectic alloys, wherein an increase of carbon concentration in eutectic has positive effect;
- 3) porosity of GCI castings is considerably smaller than that of DI.

The mechanism of shrinkage defects formation is still being discussed, though it is obvious that main reason for that is change in volume of alloy during cooling and phase transitions. This paper presents assessments of change in the specific volume of DI during crystallization using model of solidification based on cellular automata method [8-11].

The scope of the computer simulation of the casting microstructure has step out of the limits of previous topics [12-15].

More effectively and practically usage of the physically based mathematical models of solidification is possible today due to up-to-date more effective hardware capabilities and computational methods.

2. Model of the ductile iron solidification

The Cellular Automata – Finite Differences method (CA-FD) is one of the known methods of the simulation of microstructure formation during solidification [16,17]. In the CA microstructure modeling the outer grain shape is the result of the simulation and is not presupposed beforehand. The model development for a one-phase microstructure evolution is a subject of the numerous researches [18-25]. Model of the eutectic solidification of DI in the uniform temperature field and superimposed cooling rate is known [26].

The proposed mathematical model enhances the capabilities of the previous tools presented in [8]. This model takes into account the continuous nucleation of austenite and graphite grains from liquid controlled by the undercooling, separate non-equilibrium growth of graphite nodules and austenite dendrites at the first stage of solidification, and the following cooperative growth of graphite-austenite eutectic in the binary Fe-C system.

The numerical solution of the nonlinear Fourier equation was used for heat flow in the analyzed domains:

$$c \frac{\partial T}{\partial \tau} = \nabla(\lambda \nabla T) + q_T \quad (1)$$

where: τ is the time, λ is the thermal conductivity, c is the volumetric specific heat and q_T is the latent heat generation rate being a consequence of phase transformation.

Solute diffusion in the domains of every phase was calculated in the same manner as temperature distribution, by the numerical solution of the diffusion equation with a source term at the interface:

$$\frac{\partial C}{\partial \tau} = \nabla(D \nabla C) + q_C \quad (2)$$

where D is the solute diffusion coefficient, and C is the solute concentration in this phase.

The carbon concentration in the graphite is always equal to 1. For the “austenite-liquid” interface:

$$C_\gamma = k C_L \quad (3)$$

where k is the solute partition coefficient, and C_γ and C_L are the carbon concentrations in the austenite and liquid.

The Eqs. (1) and (2) were solved by the Finite Differences Method. The implicit scheme was used. The solution to Eq. (2) was obtained on the dense lattice with the same spatial step as the lattice of CA (overlapped mesh). The maximum time step of the implicit scheme for the Eq. (1) solution for the temperature field for this lattice is about 10^4 times shorter. That is why another lattice (the sparse lattice) was used with a multiple spatial step and the same time sampling. The temperature of the interface cells was calculated by linear interpolation from the nodes of the sparse lattice.

Both source functions are equal to zero outside of the interface cells. In the interface cells the values of the heat and mass sources for the finite-difference scheme are:

$$q_T = L_{\alpha \rightarrow \beta} \frac{\partial f_\beta}{\partial \tau} \quad (4)$$

$$q_C = (C_\alpha - C_\beta) \frac{\partial f_\beta}{\partial \tau} \quad (5)$$

where $L_{\alpha \rightarrow \beta}$ is the volumetric latent heat of $\alpha \rightarrow \beta$ transformation, C_α and C_β are the carbon concentrations in the vanishing and growing phases, and Δf_β is the volume fraction growth of the new phase during the time step.

Grain nucleation in industrial alloys has a heterogeneous nature. The substrates for the nucleus are randomly distributed in the bulk. Bulk distribution of differently-sized substrates also has a stochastic nature. The undercooling value of substrate activation is a function of its size. Functional relationship between the active substrate fraction and undercooling ΔT should be a feature of the probability distribution law [27]. The undercooling value of each phase should be calculated relative to the appropriate liquidus lines. The number of active substrates in the domain V of the melt with an undercooling ΔT below the liquidus may be

calculated on the basis of the cumulative distribution function $F(\Delta T)$:

$$n = N_{\max} F(\Delta T)V \quad (6)$$

where: N_{\max} is the maximum specific number of substrates for nucleation.

The Weibull cumulative distribution function was used in this paper for nucleation modeling [28]:

$$F(\Delta T) = \exp(-b/\Delta T) \quad (7)$$

where b is the empirical coefficient.

The details of the numerical simulation of stochastic nucleation are described in [29]. Other details of the used CA-FD model of a two-phase eutectic solidification were introduced elsewhere [9-11,30].

Density of specific phases was determined by means of CALPHAD method [31], using Thermo-CALC[®] software. Regression equations determined by the least squares method [32] were implemented into computer model to calculate densities of each phase. The mean value of the alloy density at the steps of the solidification path was calculated as a weighted mean value of the phases density in all cells of the cellular automaton lattice. As weight coefficients the phase volume fractions were used.

3. Parameters used in calculations

Computations were carried out on a 2D grid of 640×640 cells. The side length of each CA cell was equal to 1 μm. For thermal and diffusion calculation the periodic boundary condition was used. Base cooling rate T'_{base} was assumed for the temperature field modeling setting by the following function:

$$T'_{base} = -A \exp(-B\tau) \quad (8)$$

where A and B are the empirical coefficients shown in the Table 1.

Coefficients of the Eq. (8) were determined on the base of the cooling curves obtained by mathematical modeling for DI 9 mm plate casting solidified in the green sand mold. Simulations of the prototype plates of the proper thickness were performed using the ProCAST[®] software. For the coefficients estimation the segments of the cooling curves were used out of the range of the phase transformations.

4. Results of investigation

The resulting simulation cooling curves of alloys are shown in Fig. 1. Changes in the specific volume of alloys accompanying temperature changes are shown in Fig. 2. As can be seen from this drawing, changes observed in the specific volume of the examined alloys during solidification proceed in three stages: shrinkage during cooling from the liquidus temperature γ -Fe for hypoeutectic alloys or from the C_{gr} liquidus line for hypereutectic alloys to points A1, B1 and C1, expansion in sections from A1

(B1, C1) to A2 (B2, C2) and shrinkage continuation in sections from A2 (B2, C2) to A3, (B3, C3). Points A3, B3 and C3 denote the instants when crystallization of the liquid phase is completed, and therefore shrinkage after the time marked by these points is not due to crystallization. An increase in the specific volume of the examined Fe-C alloys accompanies the eutectic crystallization and in further course of this study will be referred to as eutectic expansion (sections on the curves marked as 1-2). Accordingly, the shrinkage phenomena at an initial stage of crystallization will be referred to as pre-eutectic shrinkage, and in the final crystallization step (sections on the curves marked as 2-3) – as final shrinkage. Temperatures and times corresponding to points from A1 to C3 along with the respective volume fractions of graphite and austenite are summarized in Table 1.

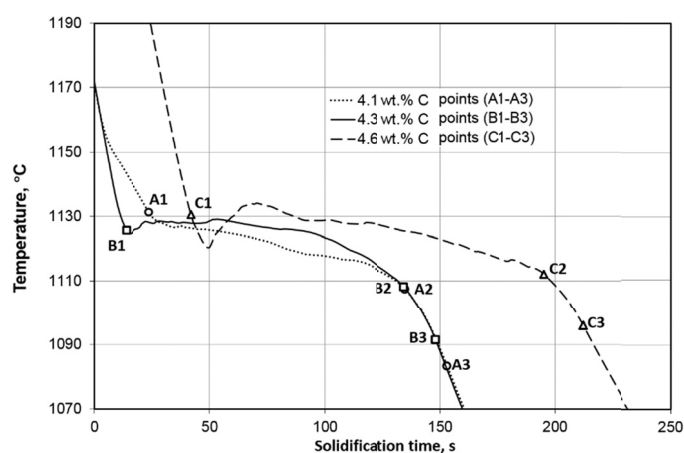


Fig. 1. Simulated cooling curves of the Fe-C alloys for different carbon contents (time measured from the instant of liquidus temperature for proper carbon content)

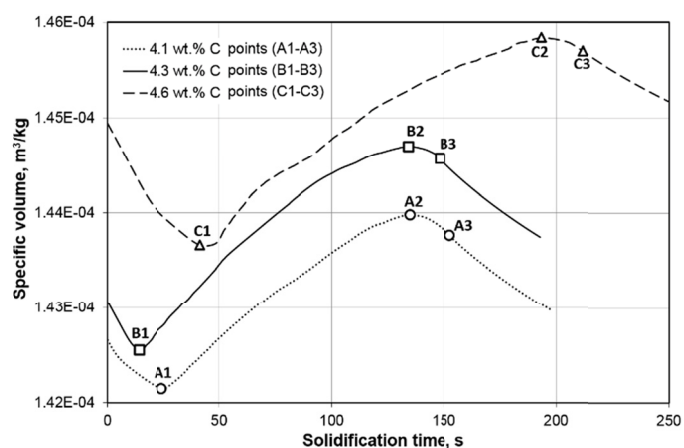


Fig. 2. Specific volume changes in the solidification time (time measured from the instant of liquidus temperature for proper carbon content)

TABLE 1

Coordinate of characteristic points A1 – C3 and volume fraction of austenite and graphite

Point	Solidification time, s	Temperature, °C	Austenite fraction	Graphite fraction
A1	24.7	1130	0.1582	0.0007
A2	135.1	1107	0.9062	0.0634
A3	153.1	1083	0.9301	0.0699
B1	14.6	1125	0.0315	0.0004
B2	134.6	1108	0.9001	0.0710
B3	149.0	1090	0.9240	0.0760
C1	42.8	1129	0.0093	0.0105
C2	194.4	1113	0.8942	0.0818
C3	212.0	1096	0.9139	0.0861

The main cause of pre-eutectic shrinkage is the decrease in the specific volume of the liquid phase accompanying the temperature drop. In hypoeutectic alloys, the additional factor is the crystallization of a phase characterized by higher density, i.e. the primary austenite whose volume fraction at the end of the pre-eutectic shrinkage approaches 0.16 (Table 1). The precipitation in hypereutectic alloys of the grains of primary graphite as a low-density phase has no major effect on the inhibition of pre-eutectic shrinkage, since at the start of eutectic shrinkage, the volume fraction of this phase exceeds only slightly the level of 0.01 (Table 1). As is apparent from Fig. 3, in the examined hypereutectic alloy, the pre-eutectic shrinkage assumes its maximum value of 0.89%, which can be explained by the greatest difference between the liquidus temperature and eutectic temperature of the alloy.

Sections A1-A2, B1-B2 and C1-C2 (Fig. 2) indicate the extent of eutectic expansion. The relative increase in specific volume at this stage of crystallization is approx. 1.3% (Fig. 3) for the hypoeutectic alloy and approx. 1.5% for the near-eutectic (4.3% C) and hypereutectic alloys. The expansion is primarily as-

sociated with a rapid growth of graphite nodules as a low-density phase. No doubt that some effect on this expansion has also the slight increase in temperature (recalescence) at the beginning of eutectic crystallization and the low rate of temperature drop after the end of recalescence.

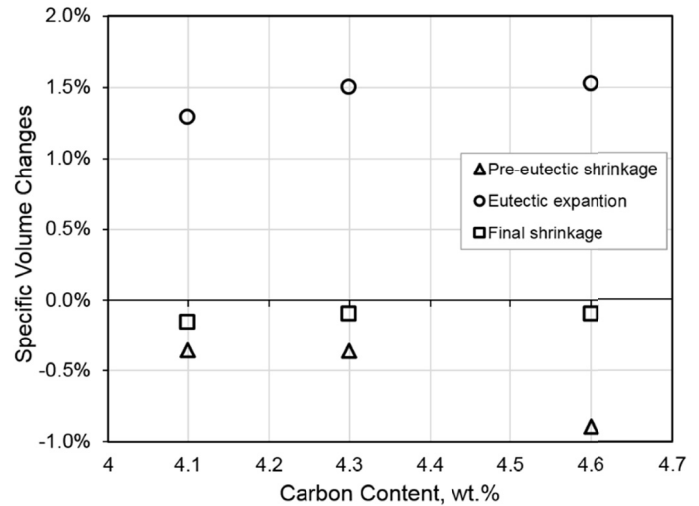


Fig. 3. Specific volume changes of the alloys during solidification for different carbon content

Fig. 4a, b show the kinetics of austenite and graphite volume fraction growth during solidification time. Visible is the earlier growth of austenite in hypoeutectic alloy (4.1 wt% C) and vice versa – the earlier growth of graphite in hypereutectic alloy (4.6 wt% C).

The state of structure at the characteristic points shown in Fig. 1-2 is reflected in the virtual microstructure shown in Fig. 5-7. The greatest differences are seen in the initial period of crystallization – Fig. 5a; Fig. 6a and Fig. 7a.

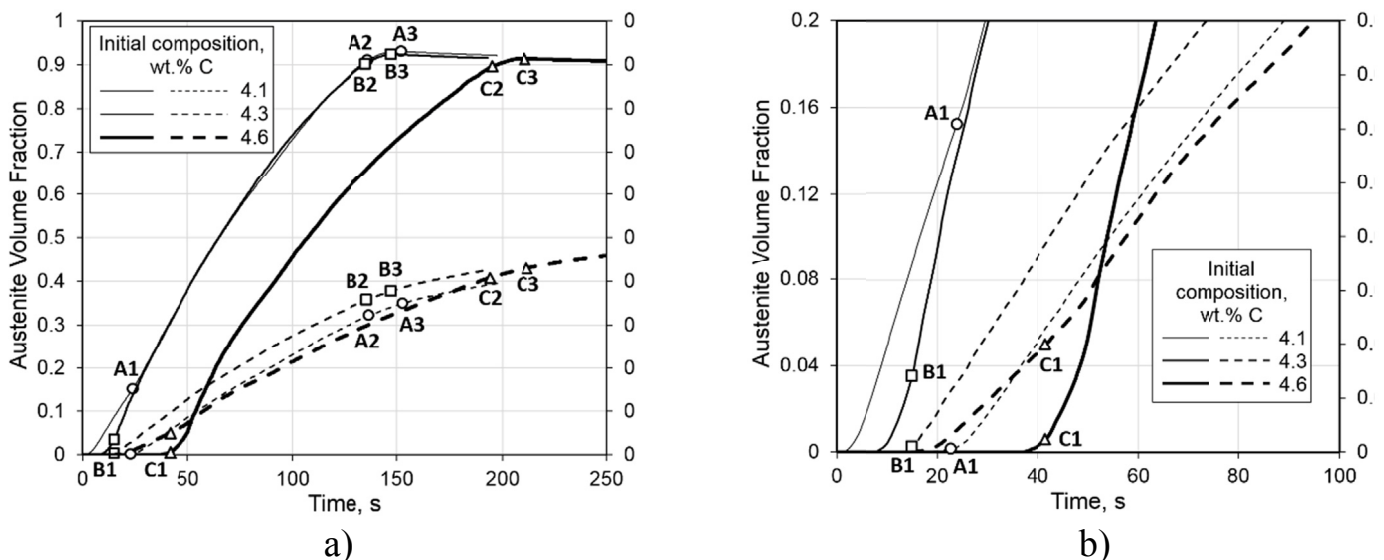


Fig. 4. Kinetics of austenite (solid lines) and graphite (dotted lines) volume fraction during solidification time (a) and for early range of time (b)

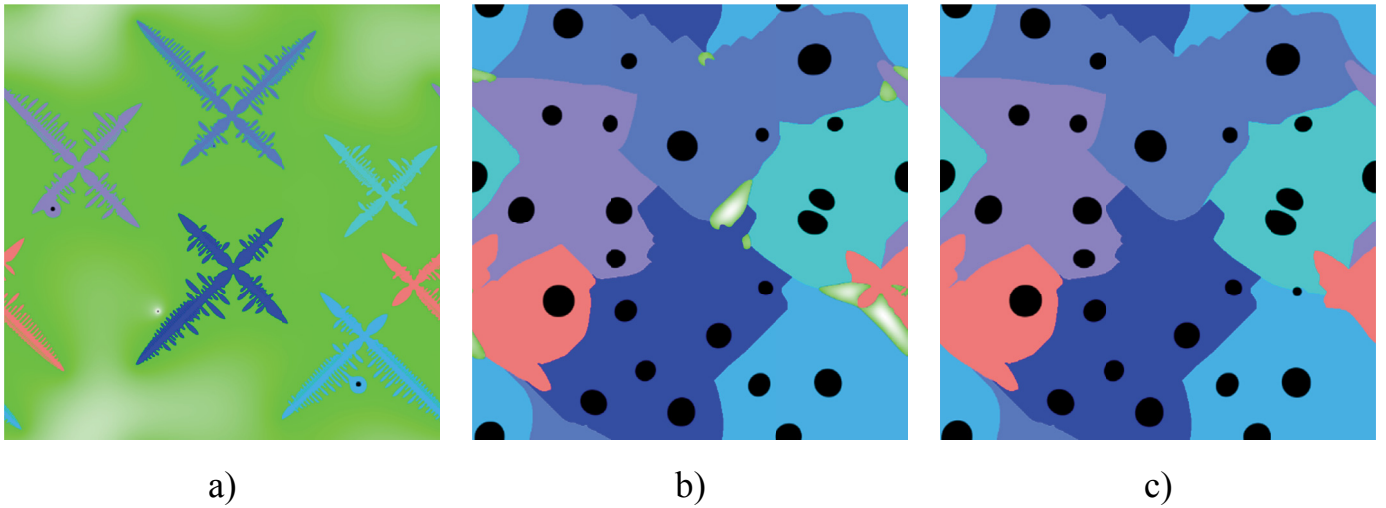


Fig. 5. Virtual microstructure calculated for carbon concentration 4.1 mass%. Solidification time, s: a) 24.7 (point A1, table 1, Fig. 1 and 2); b) 135.1 (point A2); c) 153.1 (point A3)

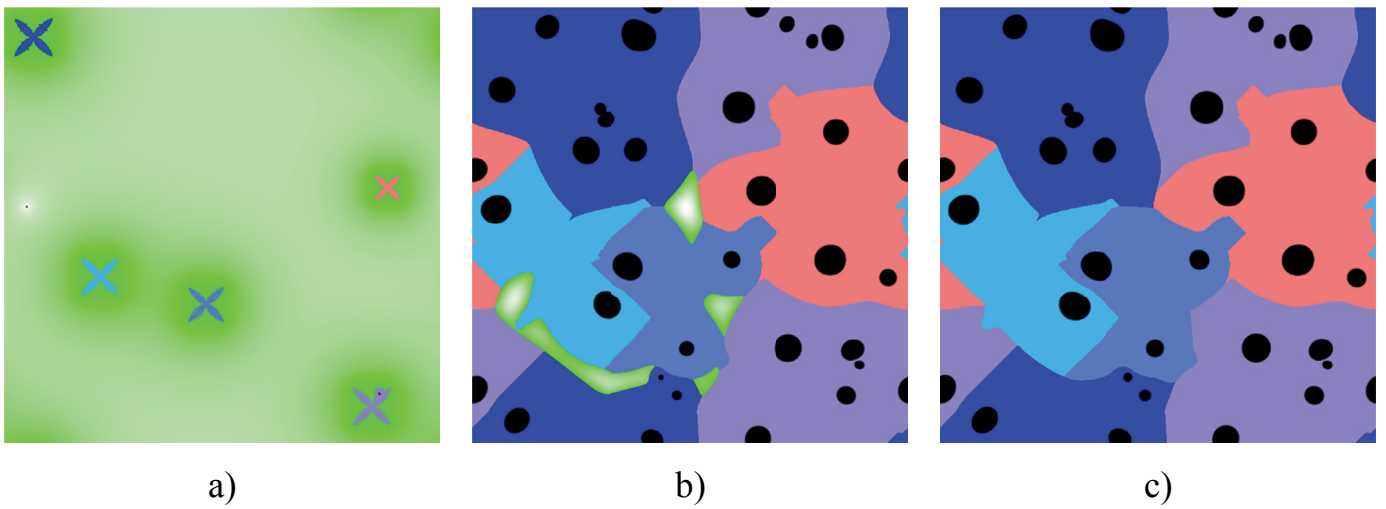


Fig. 6. Virtual microstructure calculated for carbon concentration 4.3 mass%. Solidification time, s: a) 14.6 (point B1, table 1, Fig. 1 and 2); b) 134.6 (point B2); c) 149.0 (point B3)

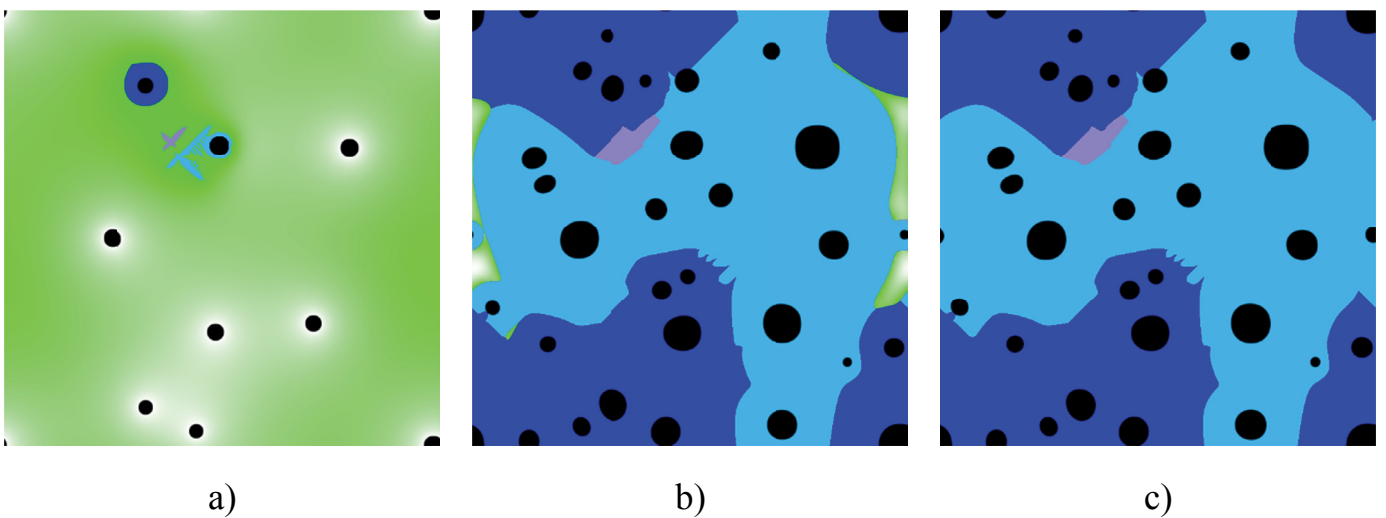


Fig. 7. Virtual microstructure calculated for carbon concentration 4.6 % mas. Solidification time, s: a) 42.8 (point C1, table 1, Fig. 1 and 2); b) 194.4 (point C2); c) 212.0 (point C3)

5. Conclusions

The DI density changes during the solidification of 9 mm thick plate castings poured in sand molds were predicted with CAFD computer model. It was shown that for all the examined compositions (4.1, 4.3 and 4.6 mass% C), the course of volumetric changes during solidification involved three stages: pre-eutectic shrinkage, expansion and final eutectic shrinkage.

The results of modeling allow better understanding of the nature and mechanism of specific volume changes in ductile iron during solidification:

- pre-eutectic shrinkage – the cause of the shrinkage are temperature-related changes in the specific volume of phases; in hypoeutectic alloys, the additional factor is the crystallization of the primary austenite grains as a phase with the lowest specific volume;
- eutectic expansion – the specific volume increases due to rapid crystallization of the grains of eutectic graphite; the alloy expansion is additionally backed up by the recalescence effect and low rate of temperature drop at the end of recalescence;
- final shrinkage – with an increasing rate of temperature drop, in the final stage of crystallization, the graphite grain growth does not compensate the shrinkage associated with the temperature-induced changes in the specific volume of phases and eutectic austenite crystallization.

The results of microstructure simulations are presented for the instant of transition from the primary shrinkage to eutectic expansion and for the instant of transition from the eutectic expansion to final shrinkage. It was shown that eutectic expansion starts before the layer of austenite can separate graphite nodules from the liquid.

Acknowledgements

This work was supported by Polish NCN project DEC-2011/01/B/ST8/01689.

REFERENCES

- [1] A. Dioszegi, L. Elmquist, J. Orlenius, I. Dugic, *Int. J. Metalcast.* **3**, 49 (2009).
- [2] I. Ohnaka, A. Sato, A. Sugiyama, F. Kinoshita, *Int. J. Cast Met. Res.* **21**, 11 (2008).
- [3] K. Weiss, Ch. Honsel, *Mat. Sci. Forum* **508**, 509 (2006).
- [4] H. Fredriksson, J. Stjerndahl, J. Tinoco, *Mat. Sci. Eng. A* **413-414**, 363 (2005).
- [5] G. Nandori, *Mat. Sci. Forum* **215-216**, 399 (1996).
- [6] The Sorelmetal Book of Ductile Iron. Rio Tinto Iron & Titanium, 2004.
- [7] Z. Gedeonova, S. Bodi, J. Dul, G. Nandori, L. Vigh, *Mat. Sci. Forum* **215-216**, 391 (1996).
- [8] A. Burbelko, E. Fraś, D. Gurgul, W. Kapturkiewicz, J. Sikora, *Key Eng. Mat.* **457**, 330 (2011).
- [9] A. Burbelko, D. Gurgul, W. Kapturkiewicz, M. Górny, *Mat. Sci. Eng.* **33**, 012083.1 (2012).
- [10] A. Burbelko, D. Gurgul, W. Kapturkiewicz, M. Górny, *Arch. Foundry Eng.* **12**, 11 (2012).
- [11] A. Burbelko, D. Gurgul, *Computer Methods in Material Science* **11**, 128 (2011).
- [12] W. Kapturkiewicz, W. Wołczyński, *Arch. Metallurgy* **37**, 149 (1992).
- [13] R. Ciach, W. Kapturkiewicz, W. Wołczyński, A.M. Zahra, *J. Therm. Anal. Calorim.* **38**, 1949 (1992).
- [14] W. Wołczyński, W. Wajda, E. Guzik, *Solid State Phenomena*, **197**, 174-179 (2013).
- [15] W. Wołczyński, E. Guzik, B. Kania, W. Wajda, *Arch. Foundry Eng.*, **9**, 254-260 (2009).
- [16] H. Rafii-Tabar, A. Chirazi, *Physics Reports-Review Section of Physics Letters* **365**, 145 (2002).
- [17] P.D. Lee, A. Chirazi, R.C. Atwood, W. Wang, *Mat. Sci. Eng. A* **365**, 57 (2004).
- [18] A.R. Umantsev, V.V. Vinogradov, V.T. Borisov, *Kristallografia* **30**, 455 (1985).
- [19] M. Rappaz, Ch.A. Gandin, *Acta Met. et Mater.* **41**, 345 (1993).
- [20] L. Nastac, D.M. Stefanescu, *Mater. Sci. Eng.* **5**, 391 (1997).
- [21] S. Pan, M. Zhu, *Acta Mater.* **58**, 340 (2010).
- [22] G. Guillemot, Ch.A. Gandin, M. Bellet, *J. Crystal Growth*, **303**, 58 (2007).
- [23] D.S. Svyetlichnyy, *Computational Materials Science* **60**, 153 (2012).
- [24] A. Burbelko, E. Fraś, W. Kapturkiewicz, D. Gurgul, *Mat. Sci. Forum* **649**, 217 (2010).
- [25] A. Burbelko, E. Fraś, W. Kapturkiewicz, E. Olejnik, *Mat. Sci. Forum* **508**, 405 (2006).
- [26] H.L. Zhao, M.F. Zhu, D.M. Stefanescu, *Key Eng. Mater.* **457**, 324 (2011).
- [27] Ch.A. Gandin, M. Rappaz, *Acta Metall. Mater.* **42**, 2233 (1994).
- [28] E. Fraś, K. Wienczek, M. Górny, H. Lopez, *Arch. Metall.* **46**, 317 (2001).
- [29] W. Kapturkiewicz, A. Burbelko, E. Fraś, M. Górny, D. Gurgul, *J. of Achievements in Materials and Manufacturing Engineering* **43**, 310 (2010).
- [30] D. Gurgul, A. Burbelko, *Arch. Met. Mater.* **55**, 53 (2010).
- [31] H.L. Lukas, S.G. Fries, B. Sundman, *Computational Thermodynamics: The Calphad Method*, Cambridge 2007.
- [32] A.A. Burbelko, D. Gurgul, M. Królikowski, M. Wróbel, *Arch. Foundry Eng.* **13**, 9-14, (2013).